Mn^{2+}-Doped CdSe/CdS Core/Multishell Colloidal Quantum Wells Enabling Tunable Carrier–Dopant Exchange Interactions

Savas Delikanli,[†,⊥] Mehmet Zafer Akgul,[†,⊥] Joseph R. Murphy,[‡,⊥] Biplob Barman,[‡] Yutsung Tsai,[‡] Thomas Scrace,[‡] Peiyao Zhang,[‡] Berkay Bozok,[†] Pedro Ludwig Hernández-Martínez,[§] Joseph Christodoulides,[∥] Alexander N. Cartwright,[‡] Athos Petrou,[*,‡] and Hilmi Volkan Demir[*,†,§]

[†]Department of Electrical and Electronics Engineering, Department of Physics, UNAM — Institute of Materials Science and Nanotechnology, Bilkent University, Ankara 06800, Turkey, [‡]Department of Physics, SUNY at Buffalo, Amherst, New York 14260, United States, [§]LUMINOUS! Center of Excellence for Semiconductor Lighting and Displays, School of Electrical and Electronic Engineering, School of Physical and Materials Sciences, Nanyang Technological University, Singapore 639798, and [∥]Naval Research Laboratory, Washington, DC 20375, United States. [⊥]S.D., M.Z.A., and J.R.M. contributed equally to this work.

ABSTRACT In this work, we report the manifestations of carrier–dopant exchange interactions in colloidal Mn^{2+}-doped CdSe/CdS core/multishell quantum wells. The carrier–magnetic ion exchange interaction effects are tunable through wave function engineering. In our quantum well heterostructures, manganese was incorporated by growing a $Cd_{0.985}Mn_{0.015}S$ monolayer shell on undoped CdSe nanoplatelets using the colloidal atomic layer deposition technique. Unlike previously synthesized Mn^{2+}-doped colloidal nanostructures, the location of the Mn ions was controlled with atomic layer precision in our heterostructures. This is realized by controlling the spatial overlap between the carrier wave functions with the manganese ions by adjusting the location, composition, and number of the CdSe, $Cd_{1-x}Mn_xS$, and CdS layers. The photoluminescence quantum yield of our magnetic heterostructures was found to be as high as 20% at room temperature with a narrow photoluminescence bandwidth of ~22 nm. Our colloidal quantum wells, which exhibit magneto-optical properties analogous to those of epitaxially grown quantum wells, offer new opportunities for solution-processed spin-based semiconductor devices.

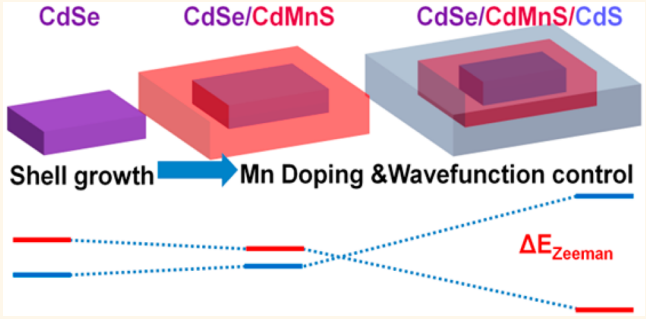

KEYWORDS: diluted magnetic semiconductors · nanoplatelets · sp–d exchange interaction · core/shell · photoluminescence

In diluted magnetic semiconductors (DMS), the incorporation of magnetic ions into a host semiconductor results in the appearance of extraordinary magnetic and optical properties.[1] The strong spin-exchange interactions between the carrier and magnetic ion spins result in these properties that can be harnessed for applications in spintronics, such as spin-polarized light-emitting diodes,[2] spin-transistors,[3] and spin-lasers.[4] Until recently, these devices have only been fabricated using molecular beam epitaxy (MBE); however, the use of colloidal nanocrystals doped with magnetic ions has attracted significant attention for these applications. Circularly polarized emission from Mn^{2+}-doped CdSe[5] and PbS[6] nanocrystals has been observed, and light-induced magnetization at room temperature has been demonstrated in $Cd_{1-x}Mn_xSe$ colloidal quantum dots (QDs).[7] In addition, the existence of carrier–dopant exchange interactions was demonstrated in Mn-doped CdSe nanoribbons.[8,9] The effects of carrier–magnetic ion spin-exchange interactions can be conveniently manipulated in core/shell heterostructures by controlling the carrier–ion wave function overlap.[10]

Colloidal quantum wells (QWs), also known as nanoplatelets (NPLs), have been synthesized recently with a thickness control at the monolayer (ML) level. This has been demonstrated in several systems including CdSe,[11,12] CdS,[13,14] and PbS.[15] Furthermore, core/shell (shell surrounding a NPL core) and

* Address correspondence to petrou@buffalo.edu, volkan@bilkent.edu.tr.

Received for review September 18, 2015 and accepted November 14, 2015.

Published online November 14, 2015
10.1021/acsnano.5b05903

core/crown (crown grown laterally around a NPL core) heterostructures were successfully synthesized by several groups.[16−19] These NPL heterostructures exhibit exceptional properties such as photoluminescence quantum yields as high as 80%,[20] spectrally narrow emission,[20] reduced fluorescence emission blinking,[18] and tunable emission.[21] The applications of NPL structures in optoelectronic devices, such as light-emitting diodes with narrower emission[22] and lasing with a low amplified spontaneous emission threshold, have been reported.[23,24] Although various NPL heterostructures have been investigated, Mn^{2+} doping of these structures and carrier−dopant exchange interactions have not been studied yet to the best of our knowledge.

Here, we report the synthesis of Mn^{2+}-doped CdSe/CdS core/shell and core/multishell NPL heterostructures and the results of room temperature optical characterization as well as a low-temperature magneto-optical study. We have demonstrated that, through wave function engineering, we can tune the effects of the sp−d exchange interaction between the carrier and Mn ion spins on the magneto-optical properties of our samples. This was accomplished by controlling the spatial overlap between the carriers and magnetic ions using colloidal atomic layer deposition (c-ALD) to grow doped or undoped layers in succession. In this work, three Mn^{2+}-doped core/shell NPL structures were synthesized by performing c-ALD deposition on 5 and 3 ML seed CdSe nanoplatelets. In each c-ALD deposition, both sides of the CdSe NPL surface were coated with 1 ML of shell material (either $Cd_{0.985}Mn_{0.015}S$ or CdS); as a result, for each cycle of shell growth, a total thickness of 2 MLs was deposited (1 ML on each of the top and bottom surfaces). A schematic of the NPL heterostructures used in this work is shown Figure 1. All five samples have a CdSe core that is surrounded by a single shell or multiple shells (composed of $Cd_{0.985}Mn_{0.015}S$ or CdS) as described in Table 1. Undoped samples 3 and 4 were used as reference samples. Doped samples 1, 2, and 5 were studied as the main part of this work for the investigation of exchange interactions between the Mn^{2+} ions and carriers. Sample 1 and sample 2 exhibit circularly polarized emission saturating around 15 and 20%, respectively, at 3 T (7 K). Magnetic sample 5, on the other hand, showed a negative spin-polarization similar to the undoped samples. In addition, samples 5, 1, and 2 exhibited Zeeman splitting of +0.5, −1.1, and −2.1 meV at 5 T (7 K), respectively. This difference in the PL circular polarization and Zeeman splitting between the doped samples is due to the difference in the spatial overlap between the carriers and Mn^{2+} ions in each sample. In addition, we determined the electron and hole wave function distribution by solving the stationary Schrödinger equation using the effective mass approximation under a strong confinement regime along the thickness of the NPL (*z*-axis). The wave functions were calculated in order to investigate the correlation between the observed behavior and the differences in the spatial overlap of the carrier wave functions with the regions containing Mn ions.

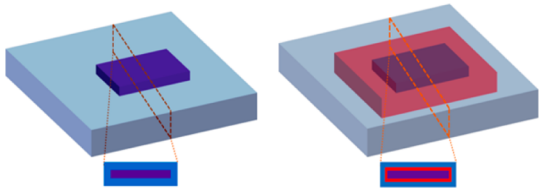

Figure 1. Illustration of the NPL heterostructure geometry. The purple region in each panel indicates the CdSe core; the red region indicates the Mn^{2+}-doped CdS shell layer, and the light blue regions correspond to the nonmagnetic CdS shell layers.

TABLE 1. List of Samples Used in This Study[a]

sample	composition
1	(5) CdSe/(2) CdMnS/(2) CdS
2	(3) CdSe/(2) CdMnS/(4) CdS
3	(5) CdSe/(2) CdS
4	(3) CdSe/(6) CdS
5	(5) CdSe/(2) CdMnS

[a] The number preceding each component of the NPL indicates the number of monolayers of that material; in all cases, the first component listed is the core and all following components are shells applied in the order listed. For shell layers, the number of monolayers is the sum of layers applied to the top and bottom of the structure.

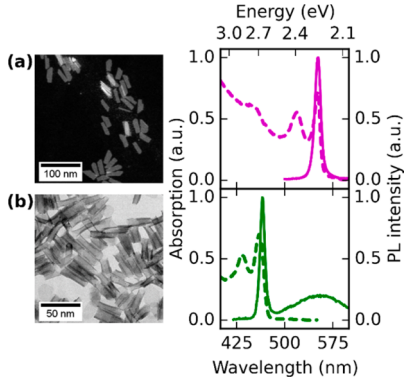

Figure 2. (Left) HAADF-TEM image of 5 ML (a) and 3 ML (b) NPL cores. (Right) Absorption (dashed lines) and photoluminescence (solid lines) of the 5 ML (a) and 3 ML (b) NPLs.

RESULTS AND DISCUSSION

High-angle annular dark-field transmission electron microscopy (HAADF-TEM) images of the 5 and 3 ML CdSe cores, used as seeds to prepare our samples, are shown in the left panels of Figure 2a,b, respectively. The 5 ML CdSe seed NPLs exhibit regular rectangular shapes having average lateral dimensions of 55 ± 6 nm × 10 ± 2 nm. It is difficult to determine the size of the 3 ML CdSe cores as they tend to fold and have irregular shapes. At room temperature, the 5 ML CdSe NPLs have a sharp emission peak at 553 nm (2.24 eV)

with a full width at half-maximum (fwhm) of 9 nm (36 meV) due to their purely 1D confinement; heavy and light hole absorption transitions occur at 552 nm (2.25 eV) and 519 nm (2.39 eV), respectively, as shown in Figure 2a (right). The band edge emission of the 3 ML CdSe NPLs occurs at 465 nm (2.67 eV), and the heavy and light hole transitions are at 460 nm (2.70 eV) and 434 nm (2.86 eV), respectively (see Figure 2b (right)).

HAADF-TEM images of sample 5, sample 1, and sample 2 are shown in the left panels of Figure 3a–c. Manganese concentration of the magnetic shell layers was determined through energy-dispersive X-ray spectroscopy (EDS) measurements, assuming that every layer in the same NPL contains the same number of atoms. Room temperature absorption and PL spectra of sample 5, sample 1, and sample 2 are shown in the right panels of Figure 3a–c. Heavy and light hole transitions of these doped NPL structures shift to longer wavelengths compared to their cores because the carrier wave functions, especially those of the electrons, extend into the CdS and CdMnS shells. The photoluminescence fwhm (approximately 22 nm, 70 meV) of these Mn^{2+}-doped core/shell NPLs is significantly narrower than that of previously reported colloidal Mn^{2+}-doped CdSe QDs which emit circularly polarized light.[5]

For the magneto-PL measurements, the NPLs were excited using the linearly polarized output of a solid state laser with a 405 nm wavelength with a maximum power density of 0.2 W/cm^2. The experiments were conducted in the Faraday geometry in which the applied magnetic field is parallel to the direction of the emitted light. The PL was analyzed into its σ_+ (left circularly polarized) and σ_- (right circularly polarized) components using a combination of a quarter-wave plate and linear analyzer placed before the spectrometer entrance slit. In Figure 4a,b, we show the PL spectra from magnetic sample 2 recorded at $T = 7$ K for magnetic fields $B = 0$ and 5 T. The shoulder on the lower energy side of the PL emission spectra taken at $T = 7$ K can be attributed to the surface traps becoming active at low temperatures, as discussed in an earlier work.[20] The difference in intensities I_+ (red) and I_- (blue) of the zero-field circularly polarized PL components is approximately zero. The circular polarization, P, is calculated using

$$P = \frac{I_+ - I_-}{I_+ + I_-} \quad (1)$$

where I_+ (I_-) is the intensity of the σ_+ (σ_-) circularly polarized PL component. For sample 2 at $B = 5$ T, $I_+ > I_-$, which results in a positive circular polarization; this is not the case for the nonmagnetic samples which exhibit negative values of P.

In our hetero-NPLs, both electrons and holes are largely localized at the central CdSe core while electron and hole wave functions penetrate by different

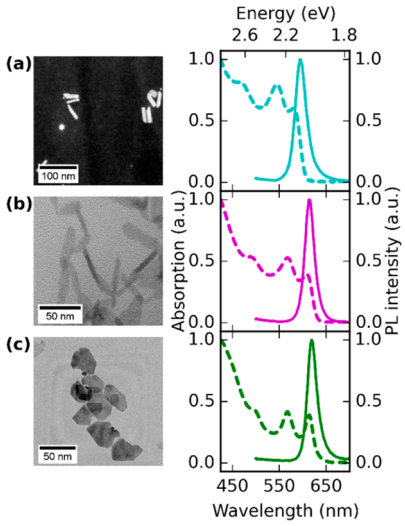

Figure 3. (Left) HAADF-TEM image of sample 5 (a), sample 1 (5) CdSe/(2) CdMnS/(2) CdS (b), and sample 2 (3) CdSe/(2) CdMnS/(4) CdS (c). (Right) Absorption (dashed lines) and PL (solid lines) of sample 5 (5) CdSe/(2) CdMnS (a), sample 1 (5) CdSe/(2) CdMnS/(2) CdS (b), and sample 2 (3) CdSe/(2) CdMnS/(4) CdS (c).

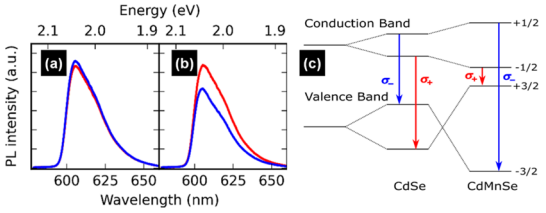

Figure 4. Photoluminescence spectra analyzed as σ_+ (red) and σ_- (blue) for sample 2 (3) CdSe/(2) CdMnS/(4) CdS, (a) $B = 0$ T; (b) $B = 5$ T. (c) Schematic diagram of the conduction and valence band edges in a zinc blende CdSe nanoplatelet. The vertical lines indicate allowed transitions of the heavy hole states in the Faraday geometry. On the left, $B = 0$ T, in the center CdSe, and right CdMnSe, $B \neq 0$ T.

amounts into the shell layers. Given this localization, the Zeeman splitting due to the sp–d interactions can be treated as the result of the electrons and holes in the CdSe core interacting with Mn^{2+} ions present in the CdMnS shell. In the doped samples, there are two contributions to the Zeeman splitting: (1) a smaller splitting due to the intrinsic electron and hole g-factors (on the order of unity) and (2) a larger conduction and valence band splitting resulting from the s–d and p–d exchange interactions. The PL emission in NPLs originates from conduction band to heavy hole transitions; a schematic of the Zeeman band splitting of the heavy hole transition in nonmagnetic and magnetic CdSe NPLs in the Faraday geometry is shown in Figure 4c. The allowed transitions, as well as their corresponding circular polarizations, are indicated by the vertical arrows. The band splittings, due to the applied magnetic field, are responsible for the energy difference between the σ_+ and σ_- transitions; this energy difference is the total Zeeman splitting, $\Delta E_Z = E(\sigma_+) - E(\sigma_-)$. According to this convention, nonmagnetic samples

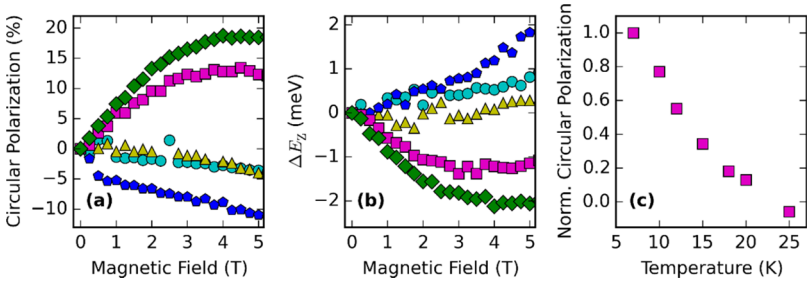

Figure 5. (a) Circular polarization of PL plotted as a function of magnetic field at T = 7 K. Data for sample 1 (5) CdSe/(2) CdMnS/(2) CdS is indicated by the magenta squares; sample 2 (3) CdSe/(2) CdMnS/(4) CdS is indicated by green diamonds; sample 3 (5) CdSe/(2) CdS is indicated by blue pentagons; sample 4 (3) CdSe/(6) CdS is indicated by yellow triangles; and sample 5 (5) CdSe/(2) CdMnS is indicated by cyan circles. (b) Zeeman splitting at T = 7 K plotted as a function magnetic field. (c) Circular polarization (normalized to the value at 7 K) of sample 1 at B = 5 T plotted as a function of temperature.

have a $\Delta E_Z > 0$, while magnetic samples exhibit negative Zeeman splitting.

The circular polarization of the PL for each of the samples is plotted as a function of magnetic field in Figure 5a. We note that there is a dramatic difference in the sign as well as the B dependence due to the incorporation of Mn ions in the shells of samples 1 and 2 when compared to the nonmagnetic samples 3 and 4. The circular polarization of sample 5, even though it contains a magnetic shell, more closely resembles the polarization behavior of the nonmagnetic sample 4. For magnetic samples 1 and 2, P increases monotonically with B up to B = 3 T; P changes little for $B > 3$ T. For the nonmagnetic reference samples, P becomes increasingly negative with increasing B. The ratio $P(T)/P(7\text{ K})$ of the circular polarizations of sample 1 at B = 5 T is plotted as a function of temperature, T, in Figure 5c. The circular polarization decreases with increasing T and changes sign between T = 20 K and T = 25 K. For this small Mn composition of the magnetic shell, this behavior is possibly due to the fact that the splitting that corresponds to g_{int} has become larger than the splitting due to sp−d exchange. The data of Figure 5a,c indicate that the magnetic shells in samples 1 and 2 are Brillouin paramagnets.[1] The PL intensity peak positions for our samples were extracted using a wavelength-weighted average of the PL spectra for the σ_+ and σ_- components. The energy difference between the two components is plotted as a function of magnetic field for sample 1 (squares), sample 2 (diamonds), sample 3 (pentagons), sample 4 (triangles), and sample 5 (circles) in Figure 5b. As in the case of P, we point out the dramatic difference in the B dependence of ΔE_Z between the nonmagnetic samples and magnetic samples 1 and 2. The Zeeman splitting of the undoped samples is positive and increases almost linearly with increasing magnetic field at 7 K. This behavior is attributed to the Zeeman splittings due to the small intrinsic hole and electron g-factors in the nonmagnetic NPLs. The Zeeman splitting of samples 1 and 2, on the other hand, is negative and has saturation values of −1.1 and −2.1 meV, respectively. We note that ΔE_Z for magnetic sample 5 more closely resembles the Zeeman splitting of the undoped samples rather than that of the doped samples; our explanation is discussed below. The Zeeman splitting can be expressed as

$$\Delta E_Z = g_{int}\mu_B B + x\langle S_z\rangle N_0(f_e\alpha - f_h\beta) \quad (2)$$

where g_{int} is the intrinsic g-factor, x is the Mn^{2+} molar fraction, $\langle S_z\rangle$ is the average value of the Mn^{2+} spin in the direction of the applied field described by the Brillouin function at low doping levels, N_0 is the cation density, α and β are the exchange constants for electron Mn^{2+} and hole Mn^{2+} spins, and f_e (f_h) describes the spatial overlap between the Mn^{2+} ions and electron (hole) wave functions.[25,26] In bulk CdMnS (CdMnSe) DMS, $N_0\alpha$ is 0.22 eV (0.23 eV) and $N_0\beta$ is −1.80 eV (−1.27 eV);[27] these exchange constants, especially α, can vary depending on quantum confinement.[28,29] The effective g-factor was calculated from our experimental data using $g_{eff} = \Delta E_Z/\mu_B B$ in the low magnetic field limit. The value of g_{eff} = 14.7 for sample 2 is an order of magnitude larger than the intrinsic g-factor of CdSe.[30]

In this section, we describe the results of electron and hole wave function calculations in our samples. The motivation is to correlate the observed magneto-optical properties (PL circular polarization and Zeeman splitting) and the spatial overlap between the carrier wave functions and the Mn ions. The calculation involves the numerical solution of the Schrödinger equation along the z-axis under the following assumptions: (1) there is no confinement in the xy plane; (2) the electron−hole Coulomb interaction is negligible; (3) the effective mass approximation is valid (effective masses were calculated following the procedure of Ithurria *et al.*[13]); and (4) infinite potential barriers exist at the external surfaces. Important parameters of the calculation are the band offsets. The offset values for our system vary widely in the literature; ΔE_{CB} ranges from −0.3 to +0.3 eV,[31−34] and ΔE_{VB} ranges from 0.4 to 0.8 eV.[35,36] For this reason, we carried out the wave function calculations using the extreme values for the offsets. Details of the calculations are provided in the Supporting Information.

We note that the calculated probabilities shown in Figure 6 are in qualitative agreement with the

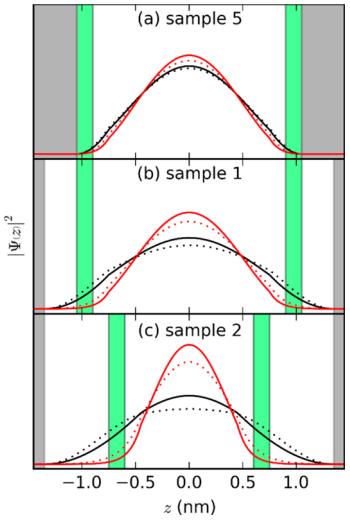

Figure 6. Square of the envelope wave function plotted as a function of the vertical dimension (*z*) for electrons (black lines) and holes (red lines). The solid lines correspond to $\Delta E_{CB} = -0.3$ eV and $\Delta E_{VB} = 0.8$ eV, and the dotted line correspond to $\Delta E_{CB} = 0.3$ eV and $\Delta E_{VB} = 0.4$ eV. Mn^{2+} ions are located in the green regions.

magneto-optical results shown in Figure 5a,b. In the case of sample 5, the magnetic shell is located exactly at the air−sample interface, and as shown in Figure 6a, the electron and hole wave function probabilities almost vanish in the vicinity of this magnetic surface layer. As shown in Figure 5a, sample 5 exhibits negative circular polarization; this behavior is similar to that of the nonmagnetic samples. The Zeeman splitting (eq 2) and thus the PL circular polarization depend strongly on the spatial overlap between the electron and hole wave functions with the Mn ions. Evidence of weak sp−d exchange interaction in sample 5 manifests itself in the Zeeman splitting, ΔE_Z, which is similar to the undoped samples, as shown in Figure 5b; this is due to the minimal spatial overlap between the Mn ions and the carrier wave functions in this structure. If we compare both the circular polarizations and Zeeman splittings of nonmagnetic sample 3 and its magnetic counterpart, sample 5, we observe that the plots of Figure 5a,b shift in the direction of magnetic sample 1.

Sample 1 was grown by depositing an undoped CdS layer on each side of sample 5. As a result, the carrier wave functions extend beyond the CdMnS shell layer, thus increasing the spatial overlap between the carriers and magnetic ions. Although the average Mn^{2+} composition decreased from 0.43 to 0.33% with the addition of the two undoped CdS layers, the Zeeman splitting changed from 0.5 to a value of approximately −1.1 meV at $B = 5$ T and $T = 7$ K. This indicates that (1) the effect of decreasing the average Mn^{2+} composition was offset by the enhancement of the carrier−Mn overlap and (2) the addition of a Mn-doped layer in sample 5 shows the emergence of weak sp−d

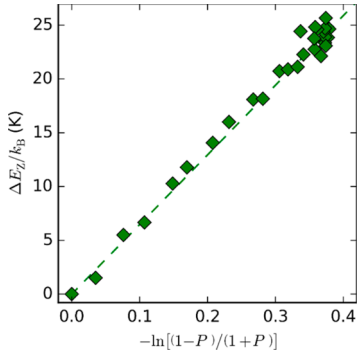

Figure 7. $\Delta E_Z/k_B$ plotted *versus* $-\ln[(1 - P)/(1 + P)]$ for sample 2 (3) CdSe/(2) CdMnS/(4) CdS. From the slope of the graph, an effective temperature of 64 K is determined.

interaction. In sample 1, this is further enhanced by the increased overlap achieved with the deposition of an outer, undoped CdS shell. In both samples 1 and 2, the average Mn^{2+} composition and the total thickness (9 ML) are the same; however, the location of the Mn^{2+}-doped layer is closer to the NPL core in sample 2, leading to correspondingly larger carrier−Mn spatial overlap. As a consequence of this, in sample 2, we observed a larger Zeeman splitting, $\Delta E_Z = -2.1$ meV at $B = 5$ T and $T = 7$ K, as shown in Figure 5b. Manganese-doped CdSe QDs with a diameter approximately the same as the thickness of our NPLs exhibit a comparable Zeeman splitting (normalized by doping percentage) when measured at similar values of H/T.[30] The discussion above points to a variety of interesting possibilities that will result in an enhancement of the exchange effects by increasing the amount of overlap between the carrier wave functions and the Mn^{2+} ions. This wave function engineering could be realized in the following forms: (1) a reduction of the core thickness, (2) an increase of the undoped, outer CdS shell thickness, and (3) the deposition of more than one magnetic CdMnS layer.

Below, we explore the dependence of P on ΔE_Z, which is given by the following equation:

$$P = \frac{1 - e^{-\Delta E_Z/k_B T_{eff}}}{1 + e^{-\Delta E_Z/k_B T_{eff}}} \quad (3)$$

where k_B is the Boltzmann constant and T_{eff} is the effective temperature of the sample. Following eq 3, we obtain a linear dependence of $\Delta E_Z/k_B$ on $-\ln[(1 - P)/(1 + P)]$ with a slope equal to T_{eff}. This relationship, which is plotted for sample 2 in Figure 7, yields a value of $T_{eff} = 64$ K. This effective temperature and the temperature, T, measured by the cryostat temperature sensor can differ due to laser heating. We expect that heating effects are stronger in our colloidal NPLs compared to MBE-grown QWs due to the fact that the latter are in intimate thermal contact with the substrate which acts as a heat sink. A similar analysis yielded an effective temperature of 54 K for sample 1 (see Supporting Information). These elevated values of

T_{eff} suggest that, for low-temperature optical studies of colloidal NPLs, heating effects must be taken into account.

CONCLUSIONS

In summary, we have demonstrated the existence of carrier−magnetic ion exchange interactions in core/multishell colloidal quantum wells using magneto-PL spectroscopy. These atomically flat core/shell NPLs having a pure thickness enabled us to study the manifestations of carrier−Mn^{2+} exchange interactions with an unprecedented control on the dopant localization. Unlike the previous works reporting Mn^{2+}-doped colloidal quantum dots earlier, which suffered from the size variation and the distribution of the dopants inside QDs, here the location of the Mn^{2+} ions can be controlled with atomic layer precision using the c-ALD technique in these NPL structures. Through the investigation of a series of doped CdSe/CdS core/shell NPLs with Mn^{2+} present in only one of the CdS shell layers, we have demonstrated that the effects of carrier−magnetic ion exchange interactions (Zeeman splitting and the resulting PL circular polarization) can be controlled by varying the spatial overlap between the wave functions of the carriers and the Mn^{2+} ions in our NPL heterostructures. Our colloidal core/shell NPLs exhibit magneto-optical properties analogous to those observed in epitaxially grown QWs. The precision of the magnetic ion location in our samples provides new prospects for solution-processed spin-based semiconductor devices.

EXPERIMENTAL SECTION

Chemicals. Cadmium nitrate tetrahydrate, sodium myristate, technical grade 1-octadecene (ODE), selenium, cadmium acetate dihydrate, manganese(II) acetate, ammonium sulfide, *N*-methylformamide (NFA), and technical grade oleic acid (OA) were purchased from Sigma-Aldrich. Methanol, ethanol, acetone, and hexane were purchased from Merck Millipore.

Preparation of Cadmium Myristate. Cadmium myristate was synthesized by following the recipe given in the literature.[18] Cadmium nitrate tetrahydrate (1.23 g) was dissolved in 40 mL of methanol, and 3.13 g of sodium myristate was dissolved in 250 mL of methanol under strong stirring; these solutions were then combined and stirred for approximately 1 h. The whitish product was centrifuged, and the white precipitate part was dissolved in methanol. This washing step with methanol was performed three times for the removal of excess precursors. Subsequently, the final whitish precipitate was kept under vacuum 24 h for drying.

Synthesis of 5 ML Thick CdSe NPLs. The 5 ML CdSe NPLs were synthesized following a recipe in the literature.[13] Cadmium myristate (170 mg) and 14 mL of ODE were loaded into three-neck flask and degassed for an hour at room temperature. Then, the solution was heated to 250 °C under a blanket of argon, and a solution of 12 mg of Se dispersed in 1 mL of ODE was quickly injected. Cadmium acetate dehydrate (120 mg) was added 1 min later. The solution was kept at 250 °C for 10 min, and 0.5 mL of OA was injected before being cooled to room temperature. The CdSe NPLs were precipitated with the addition of acetone and dispersed in hexane.

Synthesis of 3 ML Thick CdSe NPLs. First, 217 mg of cadmium acetate dihydrate, 2 mL of 0.15 M Se in ODE, 0.36 mL of OA, and 10 mL of ODE were loaded into a three-neck flask. Under nitrogen flow, the temperature was increased to 250 °C in 20 min and kept at 250 °C for 3 min. The temperature was then rapidly cooled to room temperature. The CdSe NPLs were precipitated with the addition of acetone and dispersed in hexane.

Deposition of CdS and CdMnS Layers on CdSe Core-Only NPLs. For the doping study, we modified the recipe of Ithurria *et al.*[16] Mn^{2+} ions were introduced as the manganese(II) acetate complex. Core CdSe NPLs were cleaned before the doping/shell coating because any leftover Cd or Se precursor will react during the first deposition cycle and cause overcoating of the NPLs. After successive cleaning steps, 1 mL of hexane solution of core CdSe NPLs and 1 mL of NFA were added. Then, S^{2-} ions were introduced by addition of ammonium sulfide precursor. After this, the color of the NPLs changed suddenly, and phase transfer from hexane to NFA occurred. Then, the NPLs were precipitated using toluene and acetonitrile. The precipitate was dissolved in 1 mL of NFA. This cleaning procedure was repeated at least two times to remove the excess precursors. Afterward, the Mn^{2+}−Cd^{2+} mixture was added for the doping. This precursor solution was prepared by mixing NFA solutions of manganese(II) acetate and cadmium nitrate tetrahydrate in a 1/9 Mn/Cd atomic ratio. The same cleaning procedure was performed to remove the unreacted precursors. Similarly, the CdS shell coating was carried out without using manganese(II) acetate solution. This step can be performed as many times as needed to reach the desired NPL shell thickness.

Conflict of Interest: The authors declare no competing financial interest.

Supporting Information Available: The Supporting Information is available free of charge on the ACS Publications website at DOI: 10.1021/acsnano.5b05903.

Details of the theoretical modeling and effective temperature analysis for sample 2 (PDF)

Acknowledgment. The authors would like to thank EU-FP7 Nanophotonics4Energy NoE, and TUBITAK EEEAG 109E002, 109E004, 110E010, 110E217, and 112E183, and NRF-RF-2009-09, NRF-CRP-6-2010-02, and A*STAR of Singapore for the financial support. H.V.D. acknowledges support from ESF-EURYI and TUBA-GEBIP. Work at the University at Buffalo was supported by NSF DMR 1305770.

REFERENCES AND NOTES

1. Furdyna, J. K. Diluted Magnetic Semiconductors. *J. Appl. Phys.* **1988**, *64*, R29–R64.
2. Jonker, B. T.; Park, Y. D.; Bennett, B. R.; Cheong, H. D.; Kioseoglou, G.; Petrou, A. Robust Electrical Spin Injection into a Semiconductor Heterostructure. *Phys. Rev. B: Condens. Matter Mater. Phys.* **2000**, *62*, 8180–8183.
3. Koo, H. C.; Kwon, J. H.; Eom, J.; Chang, J.; Han, S. H.; Johnson, M. Control of Spin Precession in a Spin-Injected Field Effect Transistor. *Science* **2009**, *325*, 1515–1518.
4. Holub, M.; Shin, J.; Saha, D.; Bhattacharya, P. Electrical Spin Injection and Threshold Reduction in a Semiconductor Laser. *Phys. Rev. Lett.* **2007**, *98*, 146603.
5. Beaulac, R.; Archer, P. I.; Liu, X.; Lee, S.; Salley, G. M.; Dobrowolska, M.; Furdyna, J. K.; Gamelin, D. R. Spin-Polarizable Excitonic Luminescence in Colloidal Mn^{2+} -Doped Cdse Quantum Dots. *Nano Lett.* **2008**, *8*, 1197–1201.
6. Long, G.; Barman, B.; Delikanli, S.; Tsung Tsai, Y.; Zhang, P.; Petrou, A.; Zeng, H. Carrier-Dopant Exchange Interactions in Mn-Doped Pbs Colloidal Quantum Dots. *Appl. Phys. Lett.* **2012**, *101*, 062410.
7. Beaulac, R.; Schneider, L.; Archer, P. I.; Bacher, G.; Gamelin, D. R. Light-Induced Spontaneous Magnetization in Doped Colloidal Quantum Dots. *Science* **2009**, *325*, 973–976.

8. Yu, J. H.; Liu, X.; Kweon, K. E.; Joo, J.; Park, J.; Ko, K.-T.; Lee, D. W.; Shen, S.; Tivakornsasithorn, K.; Son, J. S.; Park, J.-H.; Kim, Y.-W.; Hwang, G. S.; Dobrowolska, M.; Furdyna, J. K.; Hyeon, T. Giant Zeeman Splitting in Nucleation-Controlled Doped Cdse:Mn^{2+} Quantum Nanoribbons. *Nat. Mater.* **2010**, *9*, 47–53.
9. Fainblat, R.; Frohleiks, J.; Muckel, F.; Yu, J. H.; Yang, J.; Hyeon, T.; Bacher, G. Quantum Confinement-Controlled Exchange Coupling in Manganese(II)-Doped Cdse Two-Dimensional Quantum Well Nanoribbons. *Nano Lett.* **2012**, *12*, 5311–5317.
10. Vlaskin, V. A.; Beaulac, R.; Gamelin, D. R. Dopant−Carrier Magnetic Exchange Coupling in Colloidal Inverted Core/Shell Semiconductor Nanocrystals. *Nano Lett.* **2009**, *9*, 4376–4382.
11. Joo, J.; Son, J. S.; Kwon, S. G.; Yu, J. H.; Hyeon, T. Low-Temperature Solution-Phase Synthesis of Quantum Well Structured Cdse Nanoribbons. *J. Am. Chem. Soc.* **2006**, *128*, 5632–5633.
12. Ithurria, S.; Dubertret, B. Quasi 2d Colloidal Cdse Platelets with Thicknesses Controlled at the Atomic Level. *J. Am. Chem. Soc.* **2008**, *130*, 16504–16505.
13. Ithurria, S.; Tessier, M. D.; Mahler, B.; Lobo, R. P. S. M.; Dubertret, B.; Efros, A. L. Colloidal Nanoplatelets with Two-Dimensional Electronic Structure. *Nat. Mater.* **2011**, *10*, 936–941.
14. Li, Z.; Qin, H.; Guzun, D.; Benamara, M.; Salamo, G.; Peng, X. Uniform Thickness and Colloidal-Stable Cds Quantum Disks with Tunable Thickness: Synthesis and Properties. *Nano Res.* **2012**, *5*, 337–351.
15. Schliehe, C.; Juarez, B. H.; Pelletier, M.; Jander, S.; Greshnykh, D.; Nagel, M.; Meyer, A.; Foerster, S.; Kornowski, A.; Klinke, C.; Weller, H. Ultrathin Pbs Sheets by Two-Dimensional Oriented Attachment. *Science* **2010**, *329*, 550–553.
16. Ithurria, S.; Talapin, D. V. Colloidal Atomic Layer Deposition (C-Ald) Using Self-Limiting Reactions at Nanocrystal Surface Coupled to Phase Transfer between Polar and Nonpolar Media. *J. Am. Chem. Soc.* **2012**, *134*, 18585–18590.
17. Mahler, B.; Nadal, B.; Bouet, C.; Patriarche, G.; Dubertret, B. Core/Shell Colloidal Semiconductor Nanoplatelets. *J. Am. Chem. Soc.* **2012**, *134*, 18591–18598.
18. Tessier, M. D.; Spinicelli, P.; Dupont, D.; Patriarche, G.; Ithurria, S.; Dubertret, B. Efficient Exciton Concentrators Built from Colloidal Core/Crown Cdse/Cds Semiconductor Nanoplatelets. *Nano Lett.* **2014**, *14*, 207–213.
19. Kelestemur, Y.; Olutas, M.; Delikanli, S.; Guzelturk, B.; Akgul, M. Z.; Demir, H. V. Type-II Colloidal Quantum Wells: Cdse/Cdte Core/Crown Heteronanoplatelets. *J. Phys. Chem. C* **2015**, *119*, 2177–2185.
20. Tessier, M. D.; Mahler, B.; Nadal, B.; Heuclin, H.; Pedetti, S.; Dubertret, B. Spectroscopy of Colloidal Semiconductor Core/Shell Nanoplatelets with High Quantum Yield. *Nano Lett.* **2013**, *13*, 3321–3328.
21. Delikanli, S.; Guzelturk, B.; Hernández-Martínez, P. L.; Erdem, T.; Kelestemur, Y.; Olutas, M.; Akgul, M. Z.; Demir, H. V. Continuously Tunable Emission in Inverted Type-I Cds/Cdse Core/Crown Semiconductor Nanoplatelets. *Adv. Funct. Mater.* **2015**, *25*, 4282–4289.
22. Chen, Z.; Nadal, B.; Mahler, B.; Aubin, H.; Dubertret, B. Quasi-2d Colloidal Semiconductor Nanoplatelets for Narrow Electroluminescence. *Adv. Funct. Mater.* **2014**, *24*, 295–302.
23. Guzelturk, B.; Kelestemur, Y.; Olutas, M.; Delikanli, S.; Demir, H. V. Amplified Spontaneous Emission and Lasing in Colloidal Nanoplatelets. *ACS Nano* **2014**, *8*, 6599–6605.
24. She, C.; Fedin, I.; Dolzhnikov, D. S.; Demortière, A.; Schaller, R. D.; Pelton, M.; Talapin, D. V. Low-Threshold Stimulated Emission Using Colloidal Quantum Wells. *Nano Lett.* **2014**, *14*, 2772–2777.
25. Archer, P. I.; Santangelo, S. A.; Gamelin, D. R. Inorganic Cluster Syntheses of TM^{2+}-Doped Quantum Dots (Cdse, Cds, Cdse/Cds): Physical Property Dependence on Dopant Locale. *J. Am. Chem. Soc.* **2007**, *129*, 9808–9818.
26. Bussian, D. A.; Crooker, S. A.; Yin, M.; Brynda, M.; Efros, A. L.; Klimov, V. I. Tunable Magnetic Exchange Interactions in Manganese-Doped Inverted Core-Shell Znse-Cdse Nanocrystals. *Nat. Mater.* **2009**, *8*, 35–40.
27. Furdyna, J. K.; Kossut, J. *Diluted Magnetic Semiconductors*; Academic Press: New York, 1988.
28. Merkulov, I. A.; Yakovlev, D. R.; Keller, A.; Ossau, W.; Geurts, J.; Waag, A.; Landwehr, G.; Karczewski, G.; Wojtowicz, T.; Kossut, J. Kinetic Exchange between the Conduction Band Electrons and Magnetic Ions in Quantum-Confined Structures. *Phys. Rev. Lett.* **1999**, *83*, 1431.
29. Bhattacharjee, A. K. Confinement-Induced Reduction of the Effective Exchange Parameters in Semimagnetic Semiconductor Nanostructures. *Phys. Rev. B: Condens. Matter Mater. Phys.* **1998**, *58*, 15660–15665.
30. Archer, P. I.; Santangelo, S. A.; Gamelin, D. R. Direct Observation of sp−d Exchange Interactions in Colloidal Mn^{2+}- and Co^{2+}-Doped Cdse Quantum Dots. *Nano Lett.* **2007**, *7*, 1037–1043.
31. Tragercowan, C.; Parbrook, P. J.; Henderson, B.; O'Donnell, K. P. Band Alignments in Zn(Cd)S(Se) Strained Layer Superlattices. *Semicond. Sci. Technol.* **1992**, *7*, 536–541.
32. O'Donnell, K. P.; Parbrook, P. J.; Yang, F.; Chen, X.; Irvine, D. J.; Tragercowan, C.; Henderson, B.; Wright, P. J.; Cockayne, B. The Optical-Properties of Wide Bandgap Binary-II-VI Superlattices. *J. Cryst. Growth* **1992**, *117*, 497–500.
33. Nethercot, A. H. Prediction of Fermi Energies and Photoelectric Thresholds Based on Electronegativity Concepts. *Phys. Rev. Lett.* **1974**, *33*, 1088–1091.
34. Peng, X.; Schlamp, M. C.; Kadavanich, A. V.; Alivisatos, A. P. Epitaxial Growth of Highly Luminescent Cdse/Cds Core/Shell Nanocrystals with Photostability and Electronic Accessibility. *J. Am. Chem. Soc.* **1997**, *119*, 7019–7029.
35. Pandey, A.; Guyot-Sionnest, P. Intraband Spectroscopy and Band Offsets of Colloidal II-VI Core/Shell Structures. *J. Chem. Phys.* **2007**, *127*, 104710.
36. Li, J.; Wang, L.-W. First Principle Study of Core/Shell Structure Quantum Dots. *Appl. Phys. Lett.* **2004**, *84*, 3648–3650.